Clinical NMR Imaging of the Brain in Children: Normal and Neurologic Disease

M. A. Johnson, J. M. Pennock, G. M. Bydder, R. E. Steiner, D. J. Thomas, R. Hayward, D. R. T. Bryant, J. A. Payne, M. I. Levene, A. Whitelaw, L. M. S. Dubowitz and V. Dubowitz

AJNR Am J Neuroradiol 1983, 4 (5) 1013-1026
http://www.ajnr.org/content/4/5/1013

Clinical NMR Imaging of the Brain in Children:
Normal and Neurologic Disease

M. A. Johnson[1]
J. M. Pennock[1]
G. M. Bydder[1]
R. E. Steiner[1]
D. J. Thomas[2]
R. Hayward[2]
D. R. T. Bryant[3]
J. A. Payne[3]
M. I. Levene[4, 5]
A. Whitelaw[4]
L. M. S. Dubowitz[4]
V. Dubowitz[4]

The results of initial clinical nuclear magnetic resonance imaging of the brain in eight normal and 52 children with a wide variety of neurologic diseases were reviewed. The high level of gray-white matter contrast available with inversion-recovery sequences provided a basis for visualizing normal myelination as well as delays or deficits in this process. The appearances seen in cases of parenchymal hemorrhage, cerebral infarction, and porencephalic cysts are described. Ventricular enlargement was readily identified and marginal edema was demonstrated with spin-echo sequences. Abnormalities were seen in cerebral palsy, congenital malformations, Hallervorden-Spatz disease, aminoaciduria, and meningitis. Space-occupying lesions were identified by virtue of their increased relaxation times and mass effects. Nuclear magnetic resonance imaging has considerable potential in pediatric neuroradiologic practice, in some conditions supplying information not available by computed tomography or sonography.

In earlier reports, we commented on the potential of nuclear magnetic resonance (NMR) for imaging of the brain in children [1, 2]. The high level of gray-white matter contrast available with inversion-recovery (IR) sequences provides a basis for visualization of the normal process of myelination in infancy. Studies of adults have also shown that NMR imaging is sensitive to a variety of pathologic changes, including hemorrhage, infarction, edema, and neoplastic change, which are important in pediatric practice [1, 3–13]. Unlike computed tomography (CT), no hazard is associated with NMR imaging, and, unlike sonography, its application in children is not limited by the closure of the fontanelles. We have now completed NMR examinations of eight normal children and 52 patients up to 13 years of age with a variety of neurologic diseases. The normal appearances and results of these clinical studies are presented.

Subjects and Methods

Approval for this study was obtained from the Research Ethics Committee of the Royal Postgraduate Medical School and informed consent was obtained from a parent or guardian before examination of each child. The examinations were performed in accordance with guidelines provided by the National Radiological Protection Board [14].

The eight normal children (two boys, six girls) were aged 36 weeks postmenstrual age (PMA) (a 31 week infant examined at 5 weeks postnatal age) to 10 years; one of these children was examined twice. The 52 patients (28 boys, 24 girls) were aged 32 weeks PMA (29 weeks gestation examined at 3 weeks postnatal age) to 13 years. Their clinical diagnoses are summarized in table 1. Ten of these children had follow-up examinations. The ages of children under 2 years were corrected for prematurity or postmaturity by subtracting or adding the length of the pregnancy from 40 weeks to the patient's chronologic age.

No preparation was used in some neonates, but others and older children until the age of 4 years were sedated with oral chloral hydrate (75–100 mg/kg) or oral trimeprazine (6–8 mg/kg) 30–60 min before examination.

This article appears in the September/October 1983 issue of *AJNR* and the November 1983 issue of *AJR*.

Received April 26, 1983; accepted June 6, 1983.

M. A. Johnson is an Alberta Heritage Scholar.

[1] Department of Diagnostic Radiology, Royal Postgraduate Medical School, Hammersmith Hospital, Du Cane Rd., London W12 OHS, United Kingdom. Address reprint requests to R. E. Steiner.

[2] Institute of Neurology and National Hospital for Nervous Diseases, Queen Square, London, United Kingdom.

[3] Picker International, Wembley, Middlesex, United Kingdom.

[4] Department of Pediatrics and Neonatal Medicine, Royal Postgraduate Medical School, Hammersmith Hospital, London, United Kingdom.

[5] Present address: Department of Child Health, Leicester Medical School, Leicester, United Kingdom.

***AJNR* 4:1013–1026, September/October 1983**
0195-6108/83/0405-1013 $00.00

TABLE 1: **Clinical Diagnoses in Children Undergoing NMR of the Brain**

Diagnosis	No. Patients
Perinatal problems:	
Intraventricular hemorrhage	3
Postintraventricular hemorrhage	2
Posthemorrhagic ventricular dilatation	8
Ischemic anoxic encephalopathy	6
Subtotal	19
Congenital anomalies:	
Spina bifida with suspected Arnold-Chiari malformation	1
Aqueduct stenosis	1
Semilobar holoprosencephaly	1
Subtotal	3
Ventricular dilatation of unknown etiology	1
Metabolic abnormalities:	
Aminoaciduria	1
Congenital hypothyroidism	1
Hypernatremia	1
Fanconi disease	1
Subotal	4
Infectious diseases:	
Probable rubella embryopathy	1
Meningitis	1
Fungal abscess	1
Subtotal	3
Trauma: nonaccidental injury	1
Motor, neuromuscular, and muscular disorders:	
Familial spastic paraplegia	1
Spinomuscular atrophy	1
Hallervorden-Spatz disease	1
Congenital muscular dystrophy	2
Congenital muscular dystrophy (Fukuyama type)	1
Cerebral palsy	2
Abnormal muscle tone pattern	2
Subtotal	10
Benign tumors:	
Epidermoid	1
Hamartoma	1
Subtotal	2
Malignant tumors:	
Poorly differentiated fibrosarcoma	1
Intrinsic brainstem tumor	1
Subtotal	2
Degenerative disorders:	
Neurodegenerative disorder	3
Global retardation	1
Subtotal	4
Miscellaneous	3
Normal subjects	8
Total	60

TABLE 2: **NMR Pulse Sequences**

Scanning Sequence	Duration of Scan Cycle (msec)	τ (msec)
Saturation-recovery:		
SR_{1000}	1000	...
Inversion-recovery:		
$IR_{1400/400}$	1400	400
$IR_{1800/600}$	1800	600
$IR_{2400/800}$	2400	800
Spin-echo:		
$SE_{1040/20}$	1040	20
$SE_{1080/40}$	1080	40
$SE_{1120/60}$	1120	60
$SE_{1160/80}$	1160	80
$SE_{1240/120}$	1240	120

TABLE 3: **Dependence of NMR Image Pixel Values on ρ, T_1, and T_2 with Different Pulse Sequences**

Pulse Sequence	Image Parameters		
	ρ	T_1	T_2
Saturation-recovery	Proportional to ρ*	Reduced if T_1 is long	...
Inversion-recovery	Proportional to ρ	Decreases as T_1 increases*	...
Spin-echo	Proportional to ρ	Reduced if T_1 is long	Increases as T_2 increases*

* Indicates principal image parameter for the pulse sequence.

The duration of the examination was 45–110 min and involved up to 14 individual slices. A surface respiratory monitor was used in most children and an esophageal stethoscope was used to monitor heart rate in some neonatal patients. Care was taken to ensure that infants did not become cold during the examination.

The NMR scanner used in this study has been described [13, 15]. It is based on a cryomagnet operating at 0.15 T that induces a net proton magnetization in the long axis of the patient. Oscillating magnetic field pulses are used to perturb this magnetization. Its relaxation back to the original magnitude and direction produces an electrical signal in a receiver coil that surrounds the patient's head. Additional gradient magnetic fields are used to spatially encode the detected signal. Image reconstruction is performed by Fourier transformation and projection reconstruction or by two-dimensional Fourier transformation.

Saturation-recovery (SR), IR, and spin-echo (SE) pulse sequences were used in this study (table 2). IR sequences with τ = 600 msec were applied in neonates and infants up to 5 years of age and IR sequences with τ = 400 msec were used for older children. The pulse sequences produced images with varying dependence on proton density (ρ), T_1 and T_2 (table 3). Increased magnetic field gradients were used in neonates and younger children in order to increase the size of the image.

All neonatal patients also had cranial sonographic examinations with an ATL Mark III sector scanner with a rotating 3.5, 5, or 7 MHz transducer. Fifteen of the children also had computed tomographic (CT) scans, with a Siemens Somatom 2 whole-body scanner operating at 125 kVp and 230 mAs in 10 patients, an EMI CT 1010 head scanner in four patients, and an Elscint Exel-905 CT scanner in one patient. Contrast-enhanced CT was used in all cases of suspected mass lesions but not in a patient with muscular disease and another with probable ischemic damage.

Results

No adverse effects were noted during the course of the examinations. A central artifact consisting of a black and

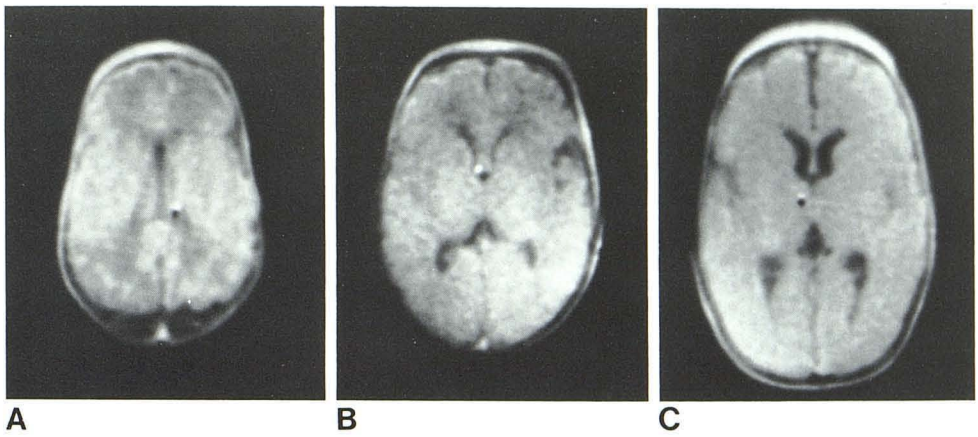

Fig. 1.—Normal SR_{1000} scans with increasing age at ventricular level. **A**, Infant born at 31 weeks gestation examined at 5 weeks postnatal age (36 weeks PMA). Ventricles identified as well as normal long T_1 areas in periventricular white matter. **B**, Full-term infant at 2 weeks postnatal age (42 weeks PMA). Long T_1 in periventricular region less prominent. **C**, Infant born at 31 weeks gestation examined at 6 months postnatal age (57 weeks PMA). Long T_1 in periventricular region no longer identified. Central artifact in each image.

white dot was present in many images, and streaks were produced at the margins of some images as a result of movement. Ventriculoatrial shunts produced image defects in their immediate vicinity.

Normal Appearances

Saturation-recovery (SR) sequences. SR sequences reflect changes in proton density with some dependence on T_1. The brain appears relatively featureless, except that in an infant of 31 weeks gestation examined at 5 weeks of age (36 weeks PMA) and in one full-term infant examined at 2 weeks of age (42 weeks PMA), long T_1 (dark) areas were seen in the periventricular regions (figs. 1A and 1B). The 36 week infant had a transient period of hypotonia shortly after birth lasting a few days, but was normal by 5 weeks postnatal age. The long T_1 in the periventricular regions was not seen in an infant of 31 weeks gestational age and examined at 6 months (57 weeks PMA) (fig. 1C) or in older children. The appearance is similar to that seen with CT where low-attenuation areas are seen in the corresponding positions.

Inversion-recovery (IR) sequences. Long T_1 areas were seen in the periventricular regions with IR scans. These were more marked than those seen with SR scans. IR images were notable for the high level of contrast between gray and white matter. Little or no white matter was seen in the neonate of 36 weeks PMA (fig. 2A), but white matter was evident within the posterior internal capsule and thalami of the infant of 42 weeks PMA (fig. 2B). In an infant born at 31 weeks gestation and examined at 6 months, white matter was present in the posterior internal capsule and thalamooccipital radiation (fig. 2C). In a full-term infant examined at 20 months the forceps minor, forceps major, and internal and external capsules were myelinated and white matter was evident in both hemispheres (fig. 2D). At 5 years more extensive myelination was seen (fig. 2E), and at 9 years the level of myelination approached that of adults (fig. 2F). The T_1 of brain in infants was longer than that in older children (table 4).

Spin-echo (SE) sequences. The ventricular system was defined but little or no gray-white matter contrast was seen with $SE_{1080/40}$ scans. The dark (long T_1) area evident with SR and IR scans was not seen in the periventricular region with this sequence (fig. 3), although with the $SE_{1160/80}$ sequence a slightly lighter (long T_2) area was seen in the periventricular region of the infant of 42 weeks PMA.

Abnormal Appearances

Intracranial hemorrhage. A parenchymal hemorrhage adjacent to the right lateral ventricle in an infant of 32 weeks gestation examined at 3 weeks postnatal age demonstrated a rim of high proton density on SR_{1000} scans. A short T_1 rim and long T_1 center were seen on $IR_{1800/600}$ scans, and a long T_2 region was seen on SE scans (fig. 4). A small subependymal hemorrhage with short T_1 was identified on the left. Ventricular dilatation was present as were areas believed to represent infarction in the right frontal and left occipital lobes. Repeat scanning 5 weeks later demonstrated resolution of the hemorrhages and decrease in the ventricular size, but persistence of the infarcts (figs. 4D–4F). A left subependymal hemorrhage was also identified as an area of short T_1 in an infant of 33 weeks gestation examined at 4 weeks postnatal age.

Infarction. Infarcts in the right frontal and left occipital lobes were identified in the infant with parenchymal hemorrhage described above (fig. 4). These were characterized by their long T_1 on $IR_{1800/600}$, $IR_{2400/800}$, and SR_{1000} scans. A third area of long T_1 was also identified in the left frontal lobe on the initial scan. This had resolved on the scan 5 weeks later and may have represented edema superimposed on the normal prolonged T_1 seen in the periventricular areas in the normal infant at 36 weeks PMA.

Porencephalic cyst. A porencephalic cyst was identified adjacent to the dilated frontal horn of the right lateral ventricle in an infant examined at 1 year of age who was born at 29 weeks gestation and who had suffered an intraventricular hemorrhage with parenchymal extension in the neonatal period.

Ventricular enlargement. Enlargement of the ventricular system was identified in 15 patients. The diagnoses in these cases were previous intraventricular hemorrhage (eight cases), aqueduct stenosis (one), ischemic anoxic encephalopathy (one), neurodegenerative disorder (one), multiple cystic periventricular leukomalacia (one), congenital muscular dystrophy (Fukuyama type) (one), aminoaciduria (one), and unknown (one).

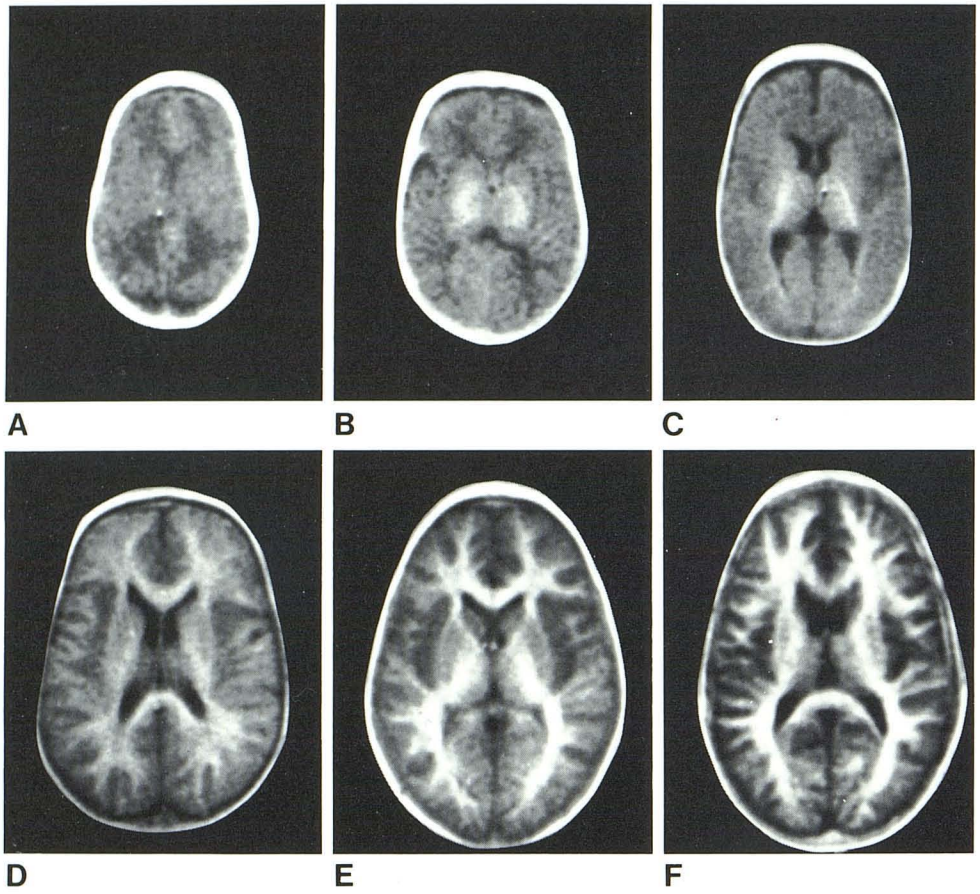

Fig. 2.—Normal IR scans with increasing age. **A**, $IR_{1800/600}$ scan in 36 week PMA infant at same level as in fig. 1A. Note prolonged T_1 in periventricular areas. **B**, $IR_{1800/600}$ scan in normal 42 week PMA infant in fig. 1B. Early myelination in posterior limb of internal capsule and thalami. Long T_1 in periventricular region less prominent. **C**, $IR_{1800/600}$ scan in normal 57 week PMA infant in fig. 1C. Extension of myelination into thalamooccipital radiation. **D**, $IR_{1800/600}$ scan. Normal 20-month-old infant. Further extension of myelination. **E**, $IR_{1400/400}$ scan. Normal 5-year-old girl. Further myelination. **F**, $IR_{1400/400}$ scan. Normal 9-year-old. Further myelination, but not yet at adult level.

TABLE 4: **Mean T_1 of Periventricular Regions and Temporal Lobes**

Age	Temporal lobes (msec)	Periventricular Region	
		Anterior (msec)	Posterior (msec)
Unmyelinated region:			
36 weeks	1000	1230	1340
42 weeks	970	1120	1060
6 months	750	780	630
Myelinated region:			
20 months	530	390	350
9 years	440	300	310

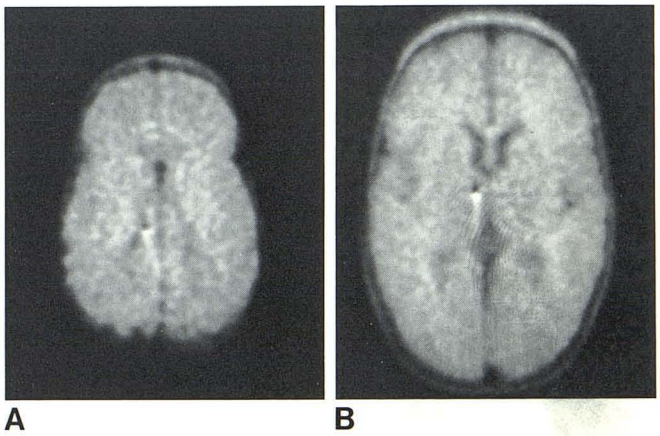

Fig. 3.—Normal $SE_{1080/40}$ scans. **A**, Normal infant born at 31 weeks gestation and examined at 5 weeks postnatal age (36 weeks PMA). Relatively featureless. **B**, Normal 57 week PMA infant.

Edema at the margin of the ventricular system was noted in five patients. This was seen as areas of prolonged T_2 surrounding the enlarged ventricles on the SE scans. In one of these patients, a repeat NMR scan after ventriculoatrial shunt placement showed reduction in the ventricular size and the degree of marginal edema (fig. 5).

Deficient or delayed myelination. White-matter development and myelination are well demonstrated with $IR_{1800/600}$ and $IR_{1400/400}$ images. Delays or deficits in myelination were diagnosed by comparison with the age-matched normal controls. When the infants were premature the chronologic age was corrected for prematurity.

Delayed or deficient myelination was recognized in four patients with previous intraventricular hemorrhage and in a single patient each with cerebral palsy, neurodegenerative

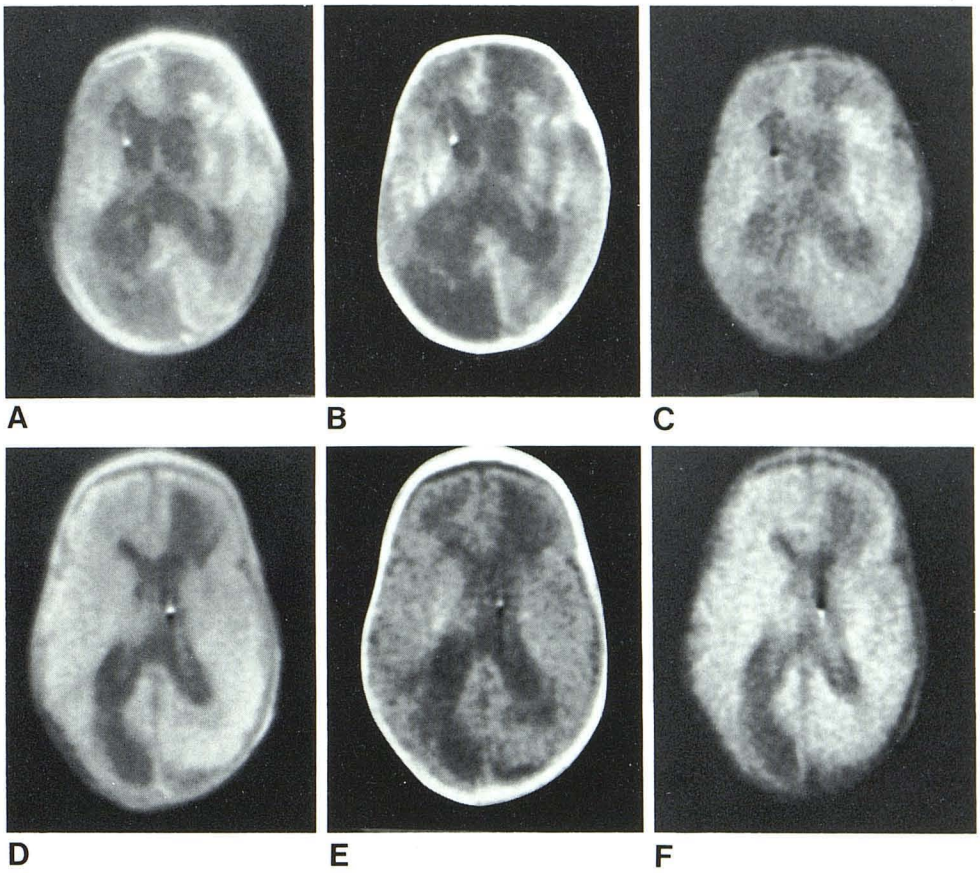

Fig. 4.—Intracerebral hematoma and infarction. Infant born at 32 weeks gestation and examined at 3 weeks postnatal age (35 weeks PMA). **A**, SR_{1000}; **B**, $IR_{1800/600}$; **C**, $SE_{1160/80}$. Right intracerebral hematoma with high proton density **(A)**, short T_1 rim and long T_1 center **(B)**, and long T_2 **(C)**. Note associated hydrocephalus, left subependymal hemorrhage, and right frontal and left occipital infarcts (long T_1) **(B)**. **D–F**, 5 weeks later. **D**, SR_{1000}; **E**, $IR_{1800/600}$; **F**, $SE_{1160/80}$. Hematoma has now resolved. Infarcts persist.

disorder, aqueduct stenosis, and probable rubella embryopathy. Ventricular dilatation was also present in three of these patients (two with intraventricular hemorrhage (fig. 6) and the other with aqueduct stenosis).

In one child born at 29 weeks gestation and examined at 14 months postnatal age with a diagnosis of posthemorrhagic hydrocephalus, delayed or deficient myelination was demonstrated when the ventriculoperitoneal shunt was malfunctioning (fig. 7). The shunt was replaced at this time with a ventriculoatrial shunt, and repeat scanning 12 months later when the shunt was functioning satisfactorily revealed myelination within the normal limits, as well as a significant decrease in ventricular size. Loss of gray-white contrast and an increase in T_1 and T_2 were seen at the anterolateral angle of the left lateral ventricle, probably indicating infarction. At this stage the child was at the expected level of clinical development for her age apart from a mild right paresis (figs. 7C and 7D).

Another patient born at 30 weeks gestation and examined at 15 months postnatal age (12½ months PMA) had a diagnosis of shunted posthemorrhagic hydrocephalus with global retardation. Myelination appeared normal, the ventricles were enlarged, and mild periventricular edema was present (fig. 8A). A repeat scan 11 months later (at 23½ months PMA) revealed deficient myelination in addition to ventricular enlargement (fig. 8B). At this time, the child demonstrated developmental delay and was behaving at about a 13 month level.

Ischemic anoxic encephalopathy. Five patients with this diagnosis were scanned. Three of these infants were full-term and were scanned at 1–2 weeks postnatal age. Two of these infants demonstrated a long T_1 in the periventricular regions on $IR_{1800/600}$ scans that was more extensive than in the normal control (fig. 9). Long T_2 areas were seen in the periventricular regions on $SE_{1160/80}$ and $SE_{1240/120}$ scans and were more prominent than the areas of long T_2 identified on the $SE_{1160/80}$ scan in the normal 42 week PMA baby.

Two patients with ischemic anoxic encephalopathy in the neonatal period were scanned at 4 and 5 months postnatal age, respectively. The 4-month-old patient had a normal scan. The NMR scan in the 5-month-old patient who had suffered encephalopathy at 4 months of age demonstrated dilated ventricles with more extensive areas of long T_2 on $SE_{1080/40}$ surrounding the ventricles and extending into the white matter.

Multicystic periventricular leukomalacia. An infant born at 31 weeks gestation was scanned at 9 weeks postnatal age. He had suffered two periods of asphyxia, one at birth from which he apparently recovered and another at 5 weeks postnatal age. Sonographic studies were normal until 9

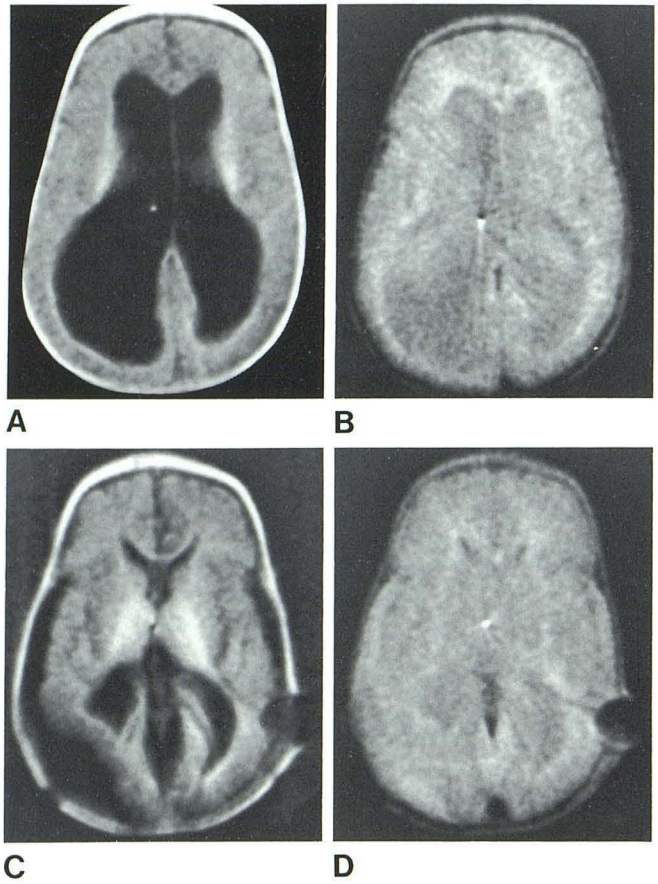

Fig. 5.—Posthemorrhagic hydrocephalus. Infant born at 29 weeks gestation, examined at 10 months postnatal age. **A**, $IR_{1800/600}$; **B**, $SE_{1120/60}$. Ventricular dilatation (**A**). Marginal edema seen as long T_2 surrounding dilated ventricles. **C** and **D**, After ventriculoatrial shunt placement. **C**, $IR_{1800/600}$; **D**, $SE_{1120/60}$. Shunt artifact, reduced ventricular size, less periventricular edema, and expansion of subarachnoid spaces now identified. Myelination normal.

Fig. 6.—Posthemorrhagic hydrocephalus at age 30 months. $IR_{1800/600}$. Delayed myelination recognized as well as ventricular dilatation and shunt artifact. (Cf. myelination with fig. 2D.)

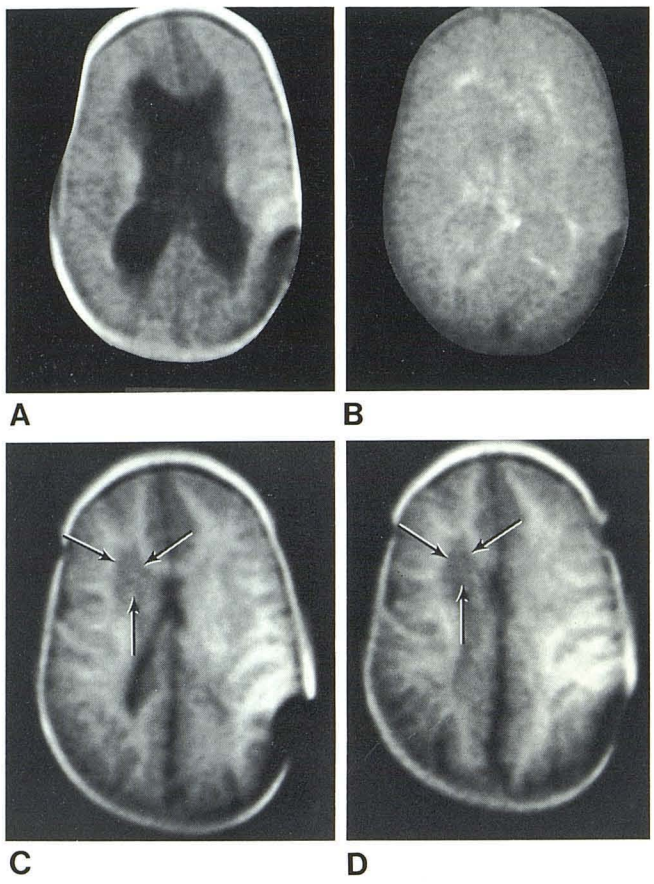

Fig. 7.—Posthemorrhagic hydrocephalus and right hemiparesis. Child born at 29 weeks gestation, examined at 14 months postnatal age. **A**, $IR_{1800/600}$; **B**, $SE_{1160/80}$. Delayed myelination. Ventricular dilatation and shunt artifact (**A**) and marginal edema (**B**). **C** and **D**, 12 months later. **C**, $IR_{1800/600}$ at high ventricular level. **D**, $IR_{1800/600}$ at supraventricular level. Reduced ventricular size. Myelination has advanced. Loss of gray-white contrast and increased T_1 at anterolateral angle of left lateral ventricle extending superiorly (*arrows*).

weeks of age, when multicystic lesions adjacent to the ventricles were demonstrated. An NMR scan at this time revealed grossly abnormal appearances with increased proton density adjacent to the lateral ventricles on SR_{1000} scans. $IR_{1800/600}$ scans revealed areas with prolonged T_1 adjacent to the mildly enlarged lateral ventricles (fig. 10). A CT scan 2 weeks after the NMR scan demonstrated moderately enlarged lateral ventricles, with adjacent low-attenuation zones. A repeat NMR scan at 8 months postnatal age displayed ventricular enlargement, possibly as a result of the cysts coalescing with the ventricular system.

Congenital malformations. A female patient with semilobar holoprosencephaly born at 35 weeks gestation was examined at 3 weeks postnatal age and again at 11 months postnatal age, and an increase in myelination was seen in the second scan (fig. 11).

Cerebral palsy of unknown etiology. A 6½-month-old patient with spastic diplegia demonstrated delayed or deficient myelination. In addition, $SE_{1160/80}$ scans demonstrated long T_2 areas in the anterior periventricular regions (fig. 12).

Muscular dystrophy. A 4-year-old patient with congenital muscular dystrophy demonstrated extensive low attenuation within the white matter on CT similar to that described in leukodystrophy. Extensive dark (long T_1) areas were identified on $IR_{1800/600}$ scans and more extensive light (long T_2)

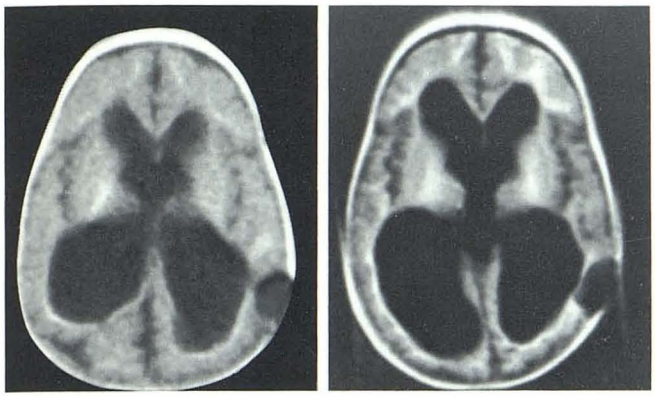

Fig. 8.—Shunted posthemorrhagic hydrocephalus. Child born at 30 weeks gestation and examined at 15 months postnatal age (12½ months PMA). **A**, $IR_{1800/600}$. Ventricular enlargement and normal myelination. **B**, 11 months later (23½ months PMA). $IR_{1800/600}$ demonstrating persistent ventricular enlargement. Myelination has advanced slightly, but is now delayed (cf. fig. 2D).

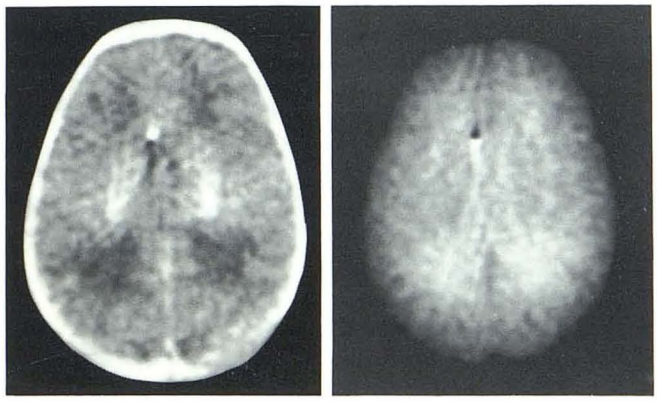

Fig. 9.—Ischemic anoxic encephalopathy. **A**, Term infant examined at 2 weeks postnatal age (42 weeks PMA). **A**, $IR_{1800/600}$. Long T_1 in periventricular areas, which is a little more extensive than normal, and early myelination. **B**, $SE_{1240/120}$. Long T_2 in periventricular region is more pronounced than normal 2-week-old. (Cf. figs. 2B and 3A, respectively.)

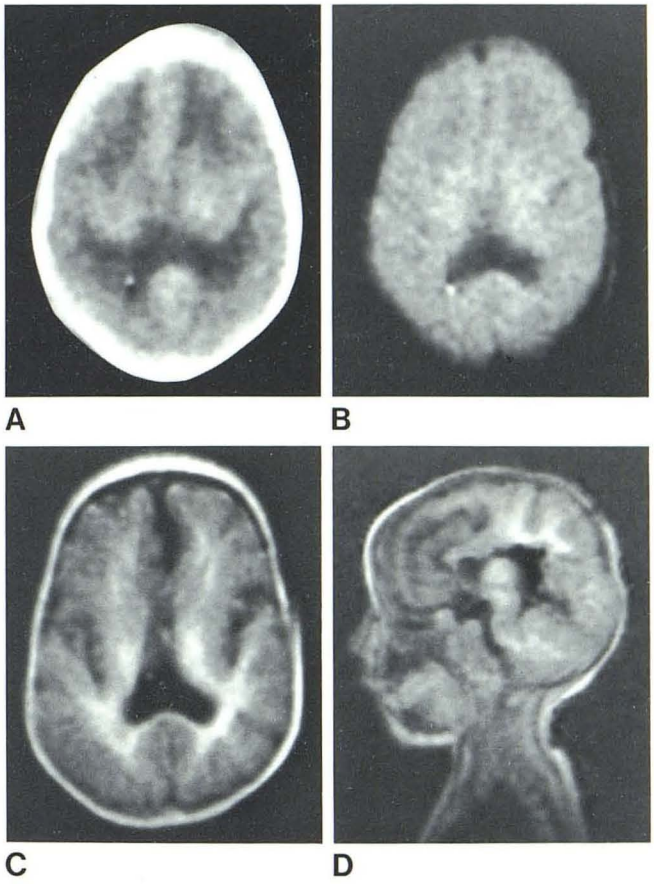

Fig. 11.—Semilobar holoprosencephaly in infant born at 35 weeks gestation and examined at 3 weeks postnatal age. **A**, $IR_{1800/600}$; **B**, $SE_{1080/40}$. Long T_1 in periventricular areas as well as early myelination in posterior limb of internal capsule. Transverse (**C**) and sagittal (**D**) $IR_{1800/600}$ scans 11 months later. Note progress of myelination and abnormal ventricular configuration.

Fig. 10.—Multicystic periventricular leukomalacia in infant born at 31 weeks gestation and examined at 9 weeks postnatal age. **A**, CT scan. Ventricular dilatation and periventricular low attenuation. SR_{1000} (**B**) and $IR_{1800/600}$ (**C**). Dark (long T_1) areas adjacent to dilated lateral ventricles.

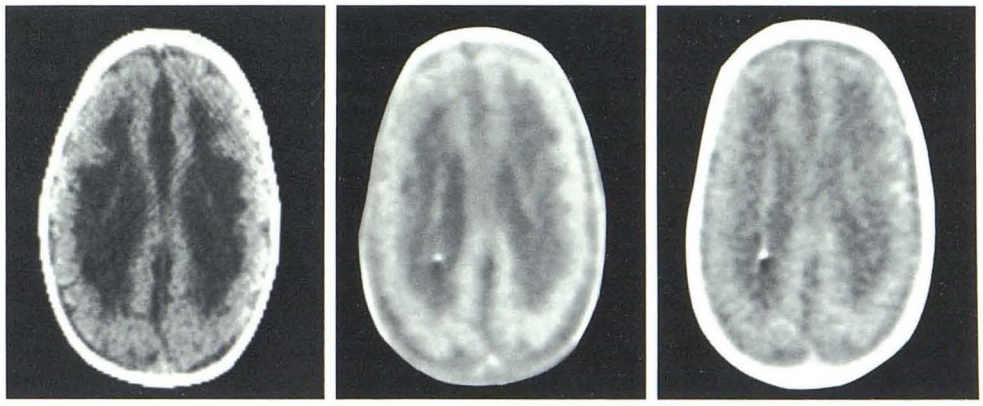

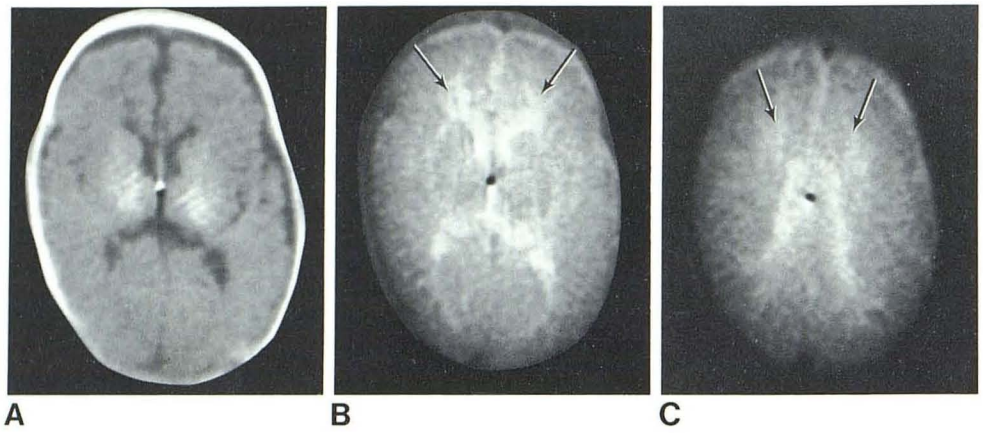

Fig. 12.—Cerebral palsy at 6½ months postnatal age. $IR_{1800/600}$ **(A)** and $SE_{1160/80}$ **(B** and **C)** at mid and high ventricular levels. Delayed myelination **(A)** and long T_2 areas in anterior periventricular regions (*arrows*, **B** and **C**).

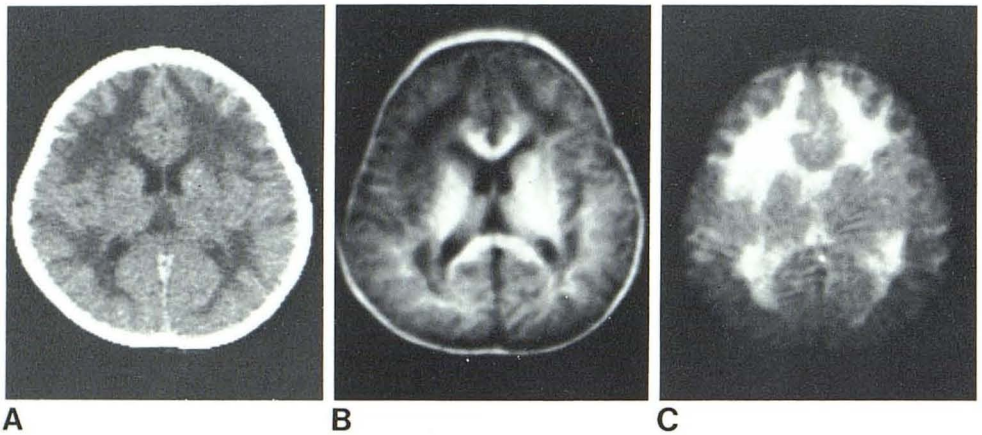

Fig. 13.—4-year-old with congenital muscular dystrophy. **A**, CT scan. **B**, $IR_{1800/600}$. Long T_1 areas in white matter. **C**, $SE_{1160/180}$. More extensive long T_2 in white matter.

areas were present on $SE_{1160/80}$ scans (fig. 13). A 4-year-old girl with congenital muscular dystrophy (Fukuyama type) also showed abnormal white matter with dark (long T_1) areas within white matter on $IR_{1800/600}$ scans. Patchy light (long T_2) areas within the white matter were identified on $SE_{1080/40}$ scans.

Subdural effusion. An 8-month-old baby who had suffered nonaccidental injury demonstrated bilateral subdural effusions in the frontal and anterior parietal zones. The effusions were identified as long T_1 areas on $IR_{1800/600}$ scans and long T_2 areas on $SE_{1240/120}$ images.

Abscess. A 13-year-old girl with aplastic anemia and bone marrow transplant developed a probable fungal abscess. Initial $IR_{1400/400}$ scans revealed a large area with variable long T_1 in the left occipital lobe and a smaller area with long T_1 in the right occipital lobe. Gray-white matter contrast was lost in the abnormal areas. Transverse and sagittal $SE_{1080/40}$ images clearly delineated the area of abnormality in the left occipital lobe (figs. 14A and 14B); it stopped abruptly at the parietooccipital junction and mainly represented edema. Within this region was an irregular rounded focus of lower T_2 representing the abscess itself. CT showed a left occipital contrast-enhancing space-occupying lesion. Histology confirmed an abscess and probable hyphae, although culture was negative. Repeat $IR_{1400/400}$ and $SE_{1080/40}$ scans 3 months after drainage of the abscess (figs. 14C and 14D) demonstrated a much smaller area of long T_1 and T_2 in the left occipital lobe with loss of gray-white matter contrast. Abnormalities in the right occipital lobe had almost completely resolved.

Extrinsic tumors. An epidermoid tumor was identified by CT in the suprasellar region of a 12-year-old girl (fig. 15). Ventricular size was normal. $IR_{1400/400}$ images revealed the tumor to be well circumscribed with short T_1 values consistent with a high lipid content. $SE_{1080/40}$ sagittal and coronal scans demonstrated long T_2 values of the tumor, as well as its relation to the brainstem. The inferior extension of the tumor was not apparent on CT.

A posterior fossa tumor identified on CT in a 9-month-old girl was studied by NMR. $IR_{1800/600}$ and $IR_{1400/400}$ images identified the lesion by its central inhomogeneous long T_1 values. $SE_{1080/40}$ and $SE_{1160/80}$ images in the transverse and sagittal planes clearly identified the lesion to arise extrinsically anterior to the brainstem, causing posterior displacement and compression of the brainstem (fig. 16). T_2 values for the tumor were inhomogeneous but slightly increased relative to the brainstem. A hypothalamic hamartoma extending into the posterior fossa was found at surgery.

Intrinsic tumors. A poorly differentiated fibrosarcoma (fig. 17) in an 8½ year-old girl was scanned. CT had identified

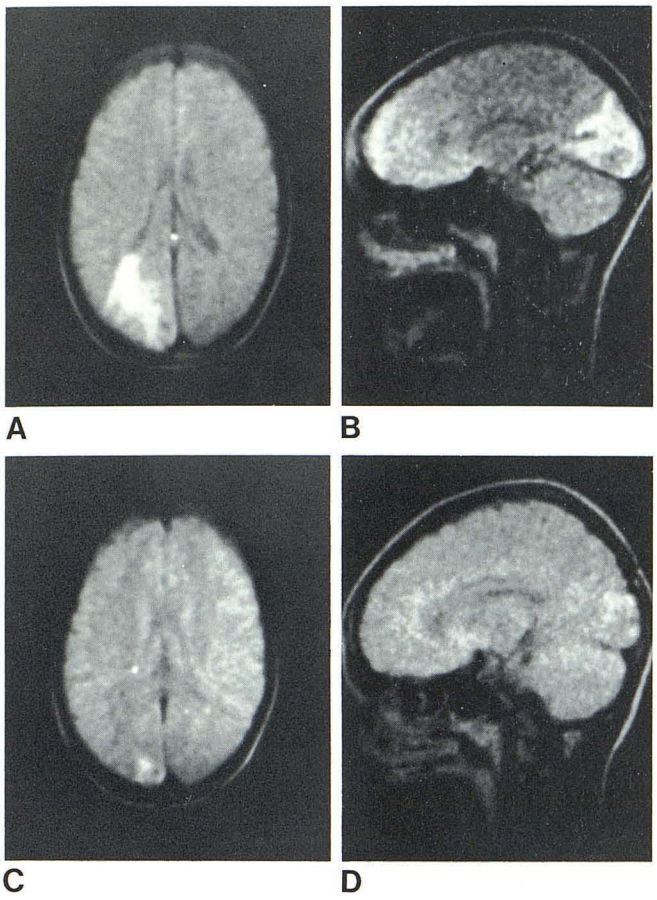

Fig. 14.—Cerebral abscess in 13-year-old before drainage. Transverse (**A**) and sagittal (**B**) $SE_{1080/40}$ scans before drainage. Extensive long T_2 in left occipital lobe (**A**) represents edema which stops abruptly at parietooccipital junction (**B**). An area of lower T_2 within edema represents abscess cavity. **C** and **D**, After drainage. Almost complete resolution of left occipital T_2 changes.

an enhancing right parietal mass lesion. $IR_{1400/400}$ images demonstrated a similar mass with an increased T_1. $SE_{1160/80}$ scans displayed the tumor with extensive surrounding edema. Internal structure was identified within the tumor and sagittal and coronal NMR scans showed more extensive change than did CT.

An intrinsic brainstem tumor in a 12-year-old patient that showed displacement of the fourth ventricle on CT was scanned (fig. 18A). $IR_{1400/400}$ images demonstrated an intrinsic lesion with long T_1 involving the brainstem and right cerebellar peduncle and hemisphere, consistent with the mass effect shown on CT. $SE_{1160/80}$ demonstrated long T_2 values within the tumor (figs. 18B and 18C).

Miscellaneous abnormal scans. A 6-year-old patient with Hallervorden-Spatz disease was scanned. $IR_{1400/400}$ images demonstrated increased T_1 regions in the lenticular nucleus. Areas of long T_2 within the basal ganglia were identified on $SE_{1160/80}$ images (fig. 19).

In a 3-month-old infant with aminoaciduria, ventricular dilatation was demonstrated. Increased T_2 areas were seen in the periventricular regions with $SE_{1160/80}$ scans. However, $SE_{1240/120}$ scans demonstrated more generalized increased T_2 values within the hemispheric white matter suggestive of cerebral edema.

In a 4-year-old girl with Fanconi disease, areas of long T_2 in the periventricular regions were noted but of uncertain significance.

The scans in an infant with meningitis who was born at 32 weeks gestation and examined at 3 weeks postnatal age showed linear areas of long T_1 extending from the frontal to occipital region on $IR_{1800/600}$ images. The changes were unusual in configuration and more extensive than the normal long T_1 areas in the periventricular regions seen in the 36-week-old normal child. The significance of this finding is uncertain, but the distribution was suggestive of watershed infarction.

A 12-year-old girl with a low-attenuation lesion with associated calcification in the right posterior parietal region on CT was also studied. An $IR_{1400/400}$ scan demonstrated a lesion in the expected location with long T_1 and associated mass effect. Repeat CT 2 months later without interval treatment demonstrated considerable resolution of this lesion, the nature of which remains uncertain.

A right temporoparietal mass lesion in a 17-month-old boy demonstrated short T_1 values on $IR_{1800/600}$ images and normal T_2 values on $SE_{1080/40}$ images suggesting a lipid-containing lesion. This was associated with dilatation and displacement of the temporal horn of the right lateral ventricle.

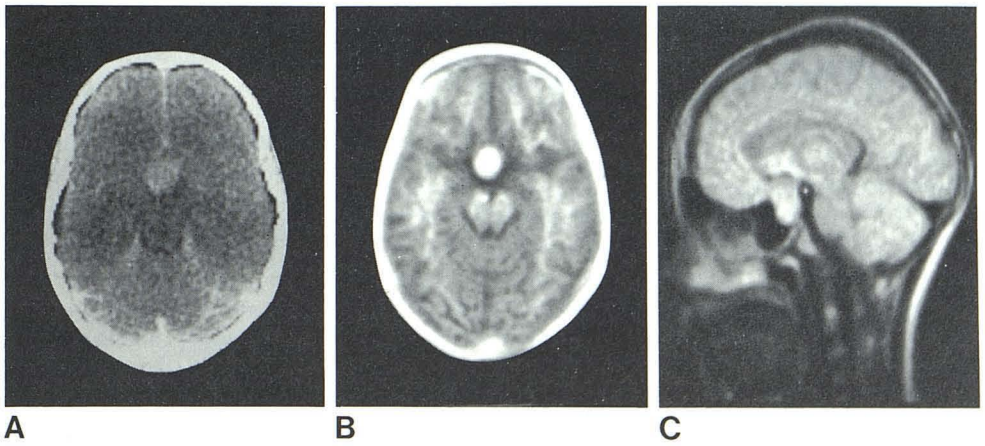

Fig. 15.—Epidermoid tumor. **A**, Contrast-enhanced CT scan. **B**, $IR_{1400/400}$. **C**, Sagittal $SE_{1080/40}$.

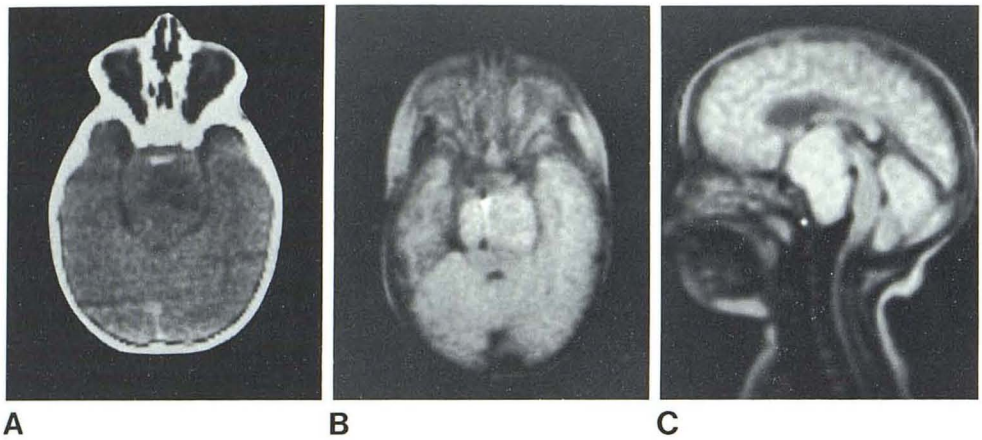

Fig. 16.—Hypothalamic hamartoma extending into posterior fossa. **A**, Contrast-enhanced CT scan. Transverse **(B)** and sagittal **(C)** $SE_{1080/80}$ NMR scans. Extrinsic lesion causes posterior displacement of brainstem.

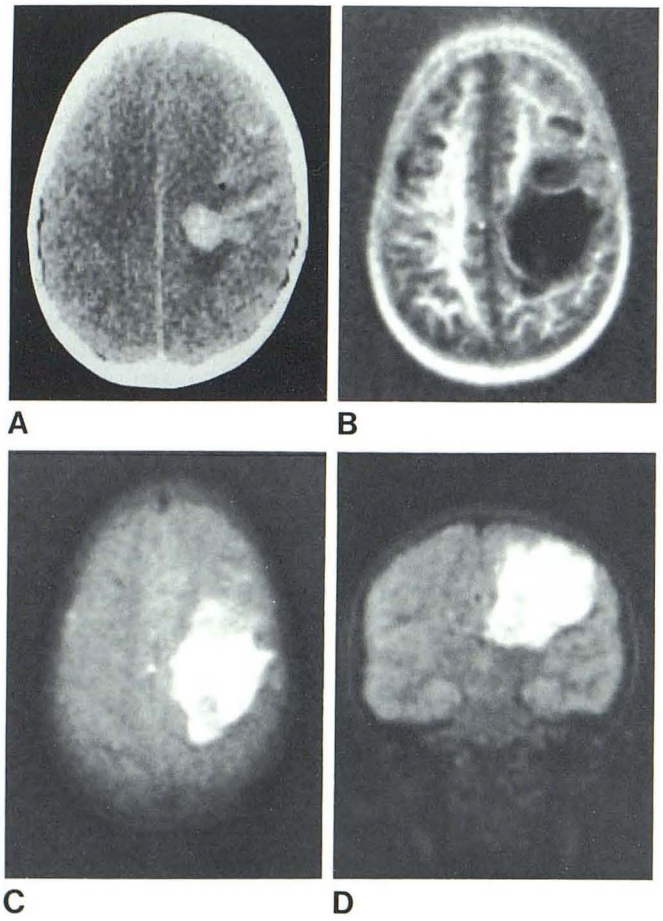

Fig. 17.—Fibrosarcoma. **A**, Contrast-enhanced CT scan. **B**, $IR_{1400/400}$ NMR scan. Mass displays long T_1 and internal structure. Transverse **(C)** and coronal **(D)** $SE_{1160/80}$ NMR scans show extensive surrounding edema.

On the basis of the NMR findings, a diagnosis of probable lipoma or hamartoma was made. Surgery was not performed.

Abnormal appearance on NMR scans was seen in an infant girl born at 35 weeks gestation who was studied at 2 weeks and at 4 months postnatal age. The findings remain of uncertain significance. The $IR_{1800/600}$ scan demonstrated extensive areas of long T_1 beyond that normally expected at 36 weeks. In addition, short T_1 and T_2 areas were present in the basal ganglia. CT demonstrated extensive low attenuation throughout both hemispheres with slight peripheral sparing. The lateral and third ventricles were not identified. Areas of increased attenuation in the basal ganglia were noted and posterior fossa structures were spared (fig. 20).

Miscellaneous patients with normal NMR findings. Intraventricular hemorrhage in an infant born at 29 weeks gestation and examined by NMR at 2 weeks postnatal age was not identified. The scans may have been made at the incorrect level or too late in the evolution of the hemorrhage. An infant born at 31 weeks gestation and examined at 6 months postnatal age who had suffered a small germinal layer hemorrhage in the neonatal period also had a normal follow-up scan. An infant who had ischemic anoxic encephalopathy associated with a choroid plexus hemorrhage in the neonatal period was scanned at 4 months postnatal age and had a normal NMR scan. A normal scan was obtained in a full-term infant examined at 6 weeks with congenital hypothyroidism. NMR was performed in a 12-year-old girl with hypernatremia to exclude a hypothalamic tumor, but none was detected. A 4-year-old with spina bifida was scanned to exclude an Arnold-Chiari malformation, and it was not demonstrated.

Normal scans were also recorded in a floppy infant born at 32 weeks gestation and examined at 2 weeks postnatal age, a full-term infant boy with cerebral palsy examined at 7 weeks, a 10-month-old infant boy with congenital muscular dystrophy, an infant girl with abnormal tone pattern who was born at 28 weeks gestation and examined at 15 months postnatal age, a 14-month-old boy with global retardation, a 26-month-old girl with a neurodegenerative disorder, and a 34-month-old boy with spinomuscular atrophy.

Discussion

The normal appearance on an NMR scan depends on the age of the patient and on the pulse sequence used. SR and IR scans demonstrate long T_1 areas in the periventricular

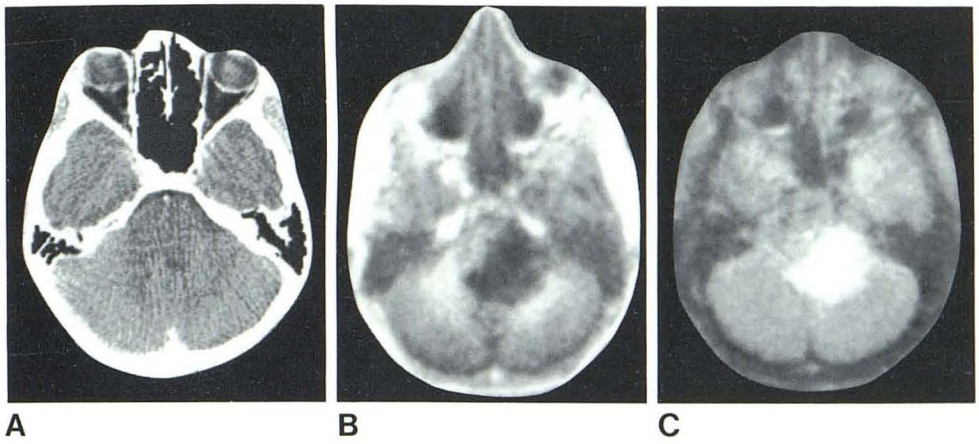

Fig. 18.—Intrinsic brainstem tumor. **A**, Contrast-enhanced CT scan. Fourth ventricle displaced. $IR_{1400/400}$ (**B**) and $SE_{1160/80}$ (**C**) NMR scans. Increased T_1 and T_2 in pons and right cerebellum.

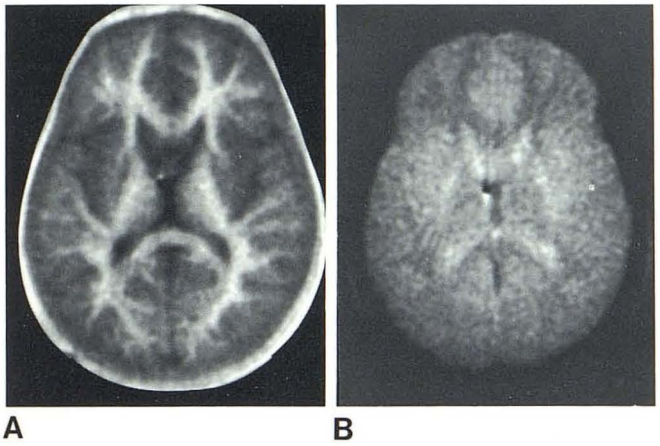

Fig. 19.—6-year-old child with Hallervorden-Spatz disease. Dark (long T_1) regions (**A**, $IR_{1400/400}$) and light (long T_2) areas (**B**, $SE_{1160/80}$) in basal ganglia.

region in neonates resolving before 6 months. This finding corresponds to the areas of low attenuation described on CT in this age group [16–19]. The water content of the brain, which ranges from 90% in the 10–34 week fetus to 72% in a child of 2 years, falls during development, while the lipid content rises [20–22]. The high water content of the neonatal brain is consistent with the finding of an increased T_1 in this age group.

The process of normal brain development has been studied extensively in vitro [20–26]. Maturation follows an orderly sequence. The extent of gyral maturation, frontal-occipital length, and degree of myelination are reliable indices of gestational age. Myelination begins in midgestation with a rapid initial phase and continues into the second decade [20–26] (fig. 21). It begins in the ventral roots of the spinal cord and proceeds cephalad. Myelination can be seen with the naked eye in the posterior internal capsule at 36 weeks gestation. The optic radiation undergoes myelination soon afterward and continues into the fourth postnatal month.

The normal infants in this study showed evidence of myelination in the posterior internal capsule at 2 weeks, in the occipitothalamic radiation at 6 months, and in the cerebral commissures and elsewhere in the hemisphere at 20 months corresponding closely to that described at postmortem. All infants who had follow-up scans showed an increase in myelination. More work will be required to determine the degree of variability of white-matter development at any age, but NMR allows physiologic myelination to be observed in vivo for the first time.

Intracranial hemorrhage is a major problem in the perinatal period [19, 22, 27]. The subependymal germinal matrix zone, which is the most common site of neonatal intracranial hemorrhage, is prominent until 32–34 weeks gestation and subsequently regresses so it is almost gone by term [22]. Subependymal hemorrhage may rupture into the ventricular system or extend peripherally into the brain resulting in intraventricular or intracerebral hemorrhage.

Subependymal hemorrhage is seen on IR scans as a short T_1 area adjacent to the lateral ventricle, and intracerebral hemorrhage demonstrates a characteristic appearance of an increased proton density, short T_1 rim with a central long T_1 on IR scans, and increased T_2 on SE scans. The long T_1 center is thought to represent central liquefaction.

The perinatal hypoxic-ischemic lesions constitute another major pediatric neurologic problem [22, 28]. NMR findings in neonates with ischemic anoxic encephalopathy suggest more extensive long T_1 and long T_2 areas in the periventricular region on SE images than seen in the normal controls, but this finding is by no means certain. Much more extensive work involving detailed comparison with normal controls will be necessary in order to be certain of the significance of these findings.

Hypoxic-ischemic lesions include periventricular leukomalacia with necrosis of the periventricular white matter at the superolateral angles of the lateral ventricles. This lesion occurs in prematures, as this area is the "watershed zone" between the central and peripheral circulation. Cavitation and thinning of the periventricular white matter may occur with associated widening of the lateral ventricles. Neurologic sequelae include spastic diplegia [22, 28].

CT has been used extensively to study neonatal ischemic anoxic encephalopathy hypoxic-ischemic lesions [16, 18, 19, 27, 29–39]. Flodmark et al. [19] compared CT and

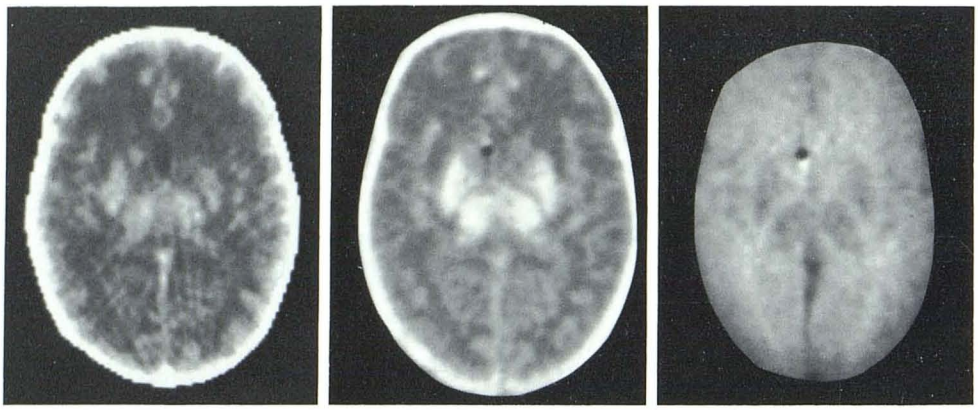

Fig. 20.—Abnormal NMR scans in infant born at 35 weeks gestation and examined at 2 weeks postnatal age (37 weeks PMA). **A**, CT scan. Extensive low attenuation throughout cerebral hemispheres with increased attenuation in basal ganglia. Long T_1 throughout cerebral hemispheres with short T_1 (**B**, $IR_{1800/600}$) and short T_2 (**C**, $SE_{1160/80}$) in basal ganglia.

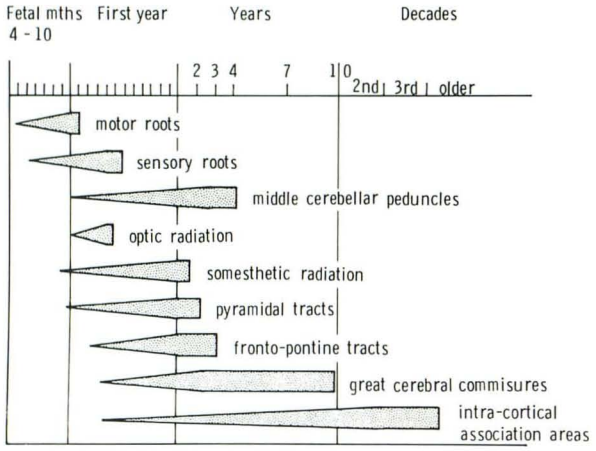

Fig. 21.—Cycles of myelination. (Adapted from [24].)

autopsy findings in infants who had suffered perinatal asphyxia and found good correlation between the CT diagnoses of supratentorial intracranial hemorrhage and cerebral edema and autopsy findings. Correlation between hypodense brain areas on CT and ischemic lesions at autopsy was poor. They believed the hypodense areas may be normal in the immature neonate, but they could also represent evidence of hypoxic brain damage. In a later study [27], they believed that decreased brain attenuation is normal in immature neonates, but it is pathologic in mature neonates, probably after 34–35 weeks.

Ventricular dilatation and porencephalic cysts are easily identified on NMR on SR and IR scans. Areas of long T_2 in the periventricular areas indicate marginal edema secondary to transependymal flow of cerebrospinal fluid. This finding suggests acute rather than chronic hydrocephalus and may be seen with shunt malfunctions. It may regress with successful treatment. Marginal edema is not seen on sonography, although ventricular size is easily assessed and may be associated with periventricular lucency on CT [40–42].

Delayed or deficient myelination is determined on NMR by comparison with myelination on IR scans in normal controls. Myelination continues until well after birth and during this phase is vulnerable to various abnormal conditions including malnutrition, inborn errors of metabolism, and rubella [22–26]. As a consequence, there is abnormal rate of myelination or abnormal myelin structure, and the subsequent evolution depends on the age and stage at which the original abnormality occurred.

The NMR findings suggest that decreased myelination is primarily due to a delay rather than a deficit in myelination. All patients who were scanned twice demonstrated increased myelination on the later scan. The clinical correlation of delays or deficits in myelination requires further study.

About half the patients with delayed or deficient myelination had dilated ventricles. The diagnosis of delayed myelination in these patients must be made cautiously, especially if there is associated marginal edema, which increases the T_1 of periventricular white matter, resulting in reduced gray-white matter contrast. In addition, periventricular white matter is compressed, making assessment of myelination more difficult.

The patient with probable rubella embryopathy was scanned at 17 months and demonstrated delay or deficit in myelination. Pathologic studies reveal that intrauterine rubella causes delayed myelination not visible until the age of 3 months and involving systems that myelinate later [22]. Delayed or deficient myelination is not evident on CT scans or sonograms and can only be demonstrated in vivo with NMR.

Two of the patients with congenital muscular dystrophy had grossly abnormal appearances of white matter T_1 and T_2 on the IR and SE scans. The appearance of the abnormal white matter in one of these patients was suggestive of leukodystrophy. Prominent white matter low attenuation on CT has been described in congenital muscular dystrophy and myopathy [43–46]. White-matter disease, which resembles spongiform degeneration, has been shown histologically in Kearns-Sayre (oculocranial somatic neuromuscular) syndrome [47, 48].

Intracranial tumors are relatively common during child-

hood, so their accurate diagnosis is important. The advent of CT scanning has led to earlier diagnosis of brain tumors in children [49], and the relatively high proportion of tumors in the posterior fossa has been noted [50–52]. Difficulties in distinguishing intrinsic and extrinsic lesions of the posterior fossa have been discussed, and the occasional subtle findings in brainstem gliomas on CT have been recognized [53, 54].

The epidermoid tumor in the suprasellar region demonstrated short T_1 values on IR scans indicating lipid content. This is an area where CT may have difficulty in making the diagnosis, as tumors may appear isodense with cerebrospinal fluid in the suprasellar cistern [55, 56].

Several miscellaneous conditions were included in which the significance of the NMR findings was uncertain. A child with aminoaciduria demonstrated prolonged hemispheric T_2 suggestive of cerebral edema. A patient with Hallervorden-Spatz syndrome, a condition associated with increased iron-containing pigment in the globus pallidus and substantia nigra, demonstrated a long T_1 region in the lenticular nucleus on IR scans and an area of long T_2 in the basal ganglia on SE scans. Associated nerve cell loss and demyelination may occur, and it is possible that the long T_2 areas represent foci of demyelination, but further study is required.

The patient born at 35 weeks gestation and examined at 2 weeks and 4 months postnatal age demonstrated extensive areas of prolonged T_1 on IR scans, as well as short T_1 and T_2 in the basal ganglia on IR and SE scans. Posterior fossa structures were spared. CT confirmed low attenuation throughout the hemispheric white matter but increased attenuation in the basal ganglia. These findings are possibly a result of extensive infarction with hemorrhage in the basal ganglia, as recently reported by Kotagal et al. [57].

NMR is the only imaging method that demonstrates myelination and allows recognition of delays or deficits. NMR can provide useful information in hemorrhagic and ischemic lesions in the newborn infant and may complement sonography especially in long-term follow-up studies. Hydrocephalus and marginal edema are readily identified on SE scans.

NMR is comparable to CT in demonstrating space-occupying lesions and has advantages over CT in posterior fossa problems. Sagittal and coronal images are especially valuable in demonstrating midline and deep-seated lesions. The variety of pulse sequences and imaging planes provides helpful additional information not available on CT.

Disadvantages of NMR include its cost, poor demonstration of calcification, and slow scanning time, although multiple-slice techniques have recently reduced scanning time [58]. Of particular interest is the recent development of a resistive magnet-based NMR machine designed specifically for pediatric use and incorporating a number of ingenious features [59, 60]. Clinical trials with this machine are awaited with considerable interest.

ACKNOWLEDGMENT

We thank the Department of Health and Social Security for generous help and acknowledge the particular contribution of Gordon Higson and John Williams.

REFERENCES

1. Bydder GM, Steiner RE, Young IR, et al. Clinical NMR imaging of the brain: 140 cases. *AJNR* **1982**;3:459–480, *AJR* **1982**;139:215–236
2. Levene MI, Whitelaw A, Dubowitz V, et al. Nuclear magnetic resonance imaging of the brain in children. *Br Med J* **1982**;285:774–776
3. Hawkes RC, Holland GN, Moore WS, Worthington BS. Nuclear magnetic resonance (NMR) tomography of the brain: a preliminary clinical assessment with demonstration of pathology. *J Comput Assist Tomogr* **1980**;4:577–586
4. Mallard J. The noes have it! Do they? *Br J Radiol* **1981**;54:831–849
5. Luiten AL, Locher PR, van Uijen C, van Dijk P, den Boef J. Clinical results of NMR imaging. In: Witcofski RL, Karstaedt N, Partain CL, eds. *NMR imaging.* Winston-Salem: Bowman Gray School of Medicine, **1982**:65–71
6. Alfidi RJ, Haaga JR, El Yousef SJ, et al. Preliminary experimental results in humans and animals with a superconducting whole-body magnetic resonance scanner. *Radiology* **1982**;143:175–181
7. Bailes DR, Young IR, Thomas DJ, Straughan K, Bydder GM, Steiner RE. NMR imaging of the brain using spin-echo sequences. *Clin Radiol* **1982**;33:395–414
8. Weinstein MA, Modic MT, Starnes DL, Pavlicek W, Gallagher J, Duchesneau PM. Nuclear magnetic resonance: comparison of inversion-recovery, saturation-recovery and usefulness of T_1 measurements of the brain in tumors (abstr). In: *Scientific program, Society of Magnetic Resonance in Medicine.* Boston: Society of Magnetic Resonance in Medicine, **1982**:152
9. Crooks LE, Mills CM, Davis PL, et al. Visualization of cerebral and vascular abnormalities by NMR imaging: the effect of imaging parameters on contrast. *Radiology* **1982**;144:843–852
10. Zeitler E, Schuierer G. NMR clinical results: Nuremburg. In: Partain CL, James AE, Rollo FD, Price RR, eds. *Nuclear magnetic resonance (NMR) imaging.* Philadephia: Saunders, **1983**:267–275
11. Buonanno FS, Pykett IL, Burt CT, et al. NMR clinical results: Massachusetts General Hospital. In: Partain CL, James AE, Rollo FD, Price RR, eds. *Nuclear magnetic resonance (NMR) imaging.* Philadelphia: Saunders, **1983**:207–230
12. Huk W, Loeffler W. NMR clinical results: Erlangen. In: Partain CL, James AE, Rollo FD, Price RR eds. *Nuclear magnetic Resonance (NMR) imaging.* Philadelphia: Saunders, **1983**:276–294
13. Bydder GM, Steiner RE, Thomas DJ, Marshall J, Gilderdale DJ, Young IR. NMR imaging of the posterior fossa: 50 cases. *Clin Radiol* **1983**;34:173–178
14. National Radiological Protection Board. *Exposure to nuclear magnetic resonance clinical imaging.* Harwell, Oxon, England: National Radiological Protection Board, **1980**
15. Young IR, Hall AS, Pallis CA, Legg NJ, Bydder GM, Steiner RE. Nuclear magnetic resonance imaging of the brain in multiple sclerosis. *Lancet* **1981**;2:1063–1066
16. Di Chiro GT. Features of premature and full-term brain: the problematic borderline between normality and pathology related to perinatal hypoxic injury. *J Comput Assist Tomogr.* **1980**;4:434
17. Brant-Zawadzki M, Enzmann DR. Using computed tomography of the brain to correlate low white-matter attenuation with early gestational age in neonates. *Radiology* **1981**;139:105–108
18. Picard L, Claudon M, Roland J, et al. Cerebral computed

tomography in premature infants with an attempt at staging developmental features. *J Comput Assist Tomogr* **1980**;4:435–444
19. Flodmark O, Becker LE, Harwood-Nash DC, Fitzhardinge PH, Fitz CR, Chuang SH. Correlation between computed tomography and autopsy in premature and full-term neonates that have suffered perinatal asphyxia. *Radiology* **1980**;137:93–103
20. Dobbing J, Sands J. Quantative growth and development of human brain. *Arch Dis Child* **1973**;48:757–767
21. Dobbings J. The later development of the brain and its vulnerability. In: Davis JA, Dobbing J, eds. *Scientific foundations of pediatrics.* London: William Heinemann Medical Books, **1981**:744–759
22. Larroche JC. *Developmental pathology of the neonate.* Amsterdam: Excepta Medica, **1977**:269–276, 283–294, 319–444
23. Lucas Keene MF, Hewer EE. Some observations on myelination in the human nervous system. *J Anat* **1931**;6:1–13
24. Yakolev PI, Lecours AR. The myelogenetic cycles of regional maturation in the brain. In: Minkowski A, ed. *Regional development of the brain in early life.* Oxford: Blackwell Scientific Publications, **1967**:3–69
25. Smith JF. *Central nervous system.* In: Berry CL, ed. *Pediatric Pathology.* Berlin: Springer-Verlag, **1981**:147–148
26. Davison AN, Peters A. *Myelination.* Springfield, IL: Thomas, **1970**:162–182
27. Flodmark O, Fitz CR, Harwood-Nash DC. CT diagnosis and short-term prognosis of intracranial hemorrhage and hypoxic/ischemic brain damage in neonates. *J Comput Assist Tomogr* **1980**;4:775–787
28. Volpe JJ. Perinatal hypoxic-ischemic brain injury. *Pediatr Clin of North Am* **1976**;23:383–397
29. Pevsner PH, Garcia-Bunnel R, Leeds N, Finklestein M. Subependymal and intraventricular hemorrhages in neonates: early diagnosis by computer tomography. *Radiology* **1976**; 119:111–114
30. Burstein J, Papile L, Burstein R. Subependymal germinal matrix and intraventricular hemorrhage in premature infants: diagnosis by CT. *AJR* **1977**;128:971–976
31. Rumack CM, McDonald MM, O'Meara OP, Sanders BB, Rudikoff JC. CT detection and course of intracranial hemorrhage in premature infants. *AJR* **1978**;131:493–497
32. Di Chiro G, Arimitsu T, Pellock JM, Landers RD. Periventricular leukomalacia related to neonatal recognition by computed tomography. *J Comput Assist Tomogr* **1978**;2:352–354
33. Burstein J, Papile L, Burstein R. Intraventricular hemorrhage and hydrocephalus in premature newborns: a prospective study with CT. *AJR* **1979**;132:631–635
34. Lee BCP, Grassi AE, Schechner S, Auld PAM. Neonatal intraventricular hemorrhage: a serial computed tomography study. *J Comput Assist Tomogr* **1979**;3:483–490
35. Schrumpf JD, Schring S, Killpack S, Brady JP, Hirata I, Mednick JP. Correlation of early neurologic outcome and CT findings in neonatal brain hypoxia and injury. *J Comput Assist Tomogr* **1980**;4:445–450
36. Hirabayashi H, Kitahara T, Hishida T. Computed tomography in perinatal hypoxic and hypoglycemic encephalopathy with emphasis on follow-up studies. *J Comput Assist Tomogr* **1980**;4:451–456
37. Magilner AD, Wertheimer IS. Preliminary results of a computed tomography study of the neonatal brain hypoxia-ischemia. *J Comput Assist Tomogr* **1980**;4:457–463
38. Flodmark O, Scott G, Harwood-Nash DC. Clinical significance of ventriculomegaly in children who suffered perinatal asphyxia with or without intracranial hemorrhage: an 18-month follow-up study. *J Comput Assist Tomogr* **1981**;5:663–673
39. Fitzhardinge PH, Flodmark O, Ashby S. The prognostic value of computed tomography of the brain in asphyxiated premature infants. *J Pediatr* **1982**;100:476–481
40. Naidich TP, Epstein F, Line JP, Kricheff II, Hochwald GM. Evaluation of pediatric hydrocephalus by computed tomography. *Radiology* **1976**;119:337–345
41. Di Chiro G, Arimitsu T, Brooks RA, et al. Computed tomography profiles of periventricular hypodensity in hydrocephalus and leukoencephalopathy. *Radiology* **1979**;130:661–666
42. Mori K, Handa H, Murata J, Yoshihisa N. Periventricular lucency in computed tomography of hydrocephalus and cerebral atrophy. *J Comput Assist Tomogr* **1980**;4:204–209
43. Kendall BE, Claveria LE, Quiroga W. CAT in leukodystrophy and neuronal degeneration. In: Du Boulay GH, Moseley IF, eds. *The first European seminar on computerized axial tomography in clinical practice.* Heidelberg: Springer, **1977**:191–202
44. Heinz ER, Drayer BP, Haenggeli CA, Painter MJ, Crumrine P. Computed tomography in white matter disease. *Radiology* **1979**;130:371–378
45. Kendall BE. Symmetrical white matter low attenuation in children. In: *X-tract No. 7.* Amsterdam: Excerpta Medica, **1979**:3–14
46. Gobernardo JM, Gimeno A. Change in cerebral white matter in a case of congenital muscular dystrophy. *Pediatr Radiol* **1982**;12:201–203
47. Seigel RS, Seeger JF, Gabrielsen TO, Allen RJ. Computed tomography in oculocranio somatic disease (Kearns-Sayre syndrome). *Neuroradiology* **1979**;130:159–164
48. Betteronini I, Engel WK, Di Chiro G, Dalakas M. Leukoencephalopathy with mitochondrial abnormalities demonstrated by computed tomgraphy. *Arch Neurol* **1979**;35:463–467
49. Tadmor R, Harwood-Nash DC, Scotti G, et al. Intracranial neoplasms in children: the effects of computed tomography on age distribution. *Radiology* **1982**;145:371–373
50. Kingsley DPA, Kendall BE. The CT scanner in posterior fossa tumors of childhood. *Br J Radiol* **1979**;52:769–776
51. Zimmerman RA, Bilaniuk LT, Bruno L, Rosenstock J. Computed tomography of cerebellar astrocytoma. *AJR* **1978**; 139:929–933
52. Bilaniuk LT, Zimmerman RA, Littman P, Gallow E, Rorke LB, Bruce DA, Schut L. Computed tomography of brain stem gliomas in children. *Radiology* **1980**;134:89–95
53. Naidich TP. Infratentorial masses. In: Norman D, Korobkin M, Newton TH, eds. *Computed tomography 1977.* San Francisco, University of California, **1977**:231–242
54. Miller EM, Newton TH. Extra-axial posterior fossa lesions stimulating intra-axial lesions on computed tomography. *Radiology* **1978**;127:675–679
55. Fawcitt HRA, Isherwood I. Radiodiagnosis of intracranial pearly tumors with particular reference to the value of computed tomography. *Neuroradiology* **1976**;11:235–242
56. Mikhael M, Mattar AG. Intracranial pearly tumors: the role of computed tomography, angiography and pneumoencephalography. *J Comput Assist Tomogr* **1978**;2:421–429
57. Kotagal S, Tore SS, Kotagal P. Archer CR. Symmetric bithalamic and striatal hemorrhage following perinatal hypoxia in a term infant. *J Comput Assist tomogr* **1983**;7:353–355
58. Crooks LE, Ortendahl DA, Kaufman L, et al. Clinical efficiency of nuclear magnetic resonance imaging. *Radiology* **1983**;146:123–128
59. Hoult DI. Rotating frame zeugmatography. *Philos Trans R Soc Lond [Biol]* **1980**;289:543–547
60. Hoult DI. NMR imaging at the National Institute of Health: a versatile electromagnet. *J Comput Assist Tomogr* **1981**; 5:291–292